


 Cite this: *RSC Adv.*, 2021, 11, 374

Thermodynamics of the double sulfates $\text{Na}_2\text{M}^{2+}(\text{SO}_4)_2 \cdot n\text{H}_2\text{O}$ ($\text{M} = \text{Mg}, \text{Mn}, \text{Co}, \text{Ni}, \text{Cu}, \text{Zn}$, $n = 2$ or 4) of the blödite–kröhnkite family†

 Juraj Majzlan,^a Delyana Marinova^b and Edgar Dachs^c

The double sulfates with the general formula $\text{Na}_2\text{M}^{2+}(\text{SO}_4)_2 \cdot n\text{H}_2\text{O}$ ($\text{M} = \text{Mg}, \text{Mn}, \text{Co}, \text{Ni}, \text{Cu}, \text{Zn}$, $n = 2$ or 4) are being considered as materials for electrodes in sodium-based batteries or as precursors for such materials. These sulfates belong structurally to the blödite ($n = 4$) and kröhnkite ($n = 2$) family and the M cations considered in this work were Mg, Mn, Co, Ni, Cu, Zn. Using a combination of calorimetric methods, we have measured enthalpies of formation and entropies of these phases, calculated their Gibbs free energies ($\Delta_f G^\circ$) of formation and evaluated their stability with respect to Na_2SO_4 , simple sulfates $\text{MSO}_4 \cdot x\text{H}_2\text{O}$, and liquid water, if appropriate. The $\Delta_f G^\circ$ values (all data in kJ mol^{-1}) are: $\text{Na}_2\text{Ni}(\text{SO}_4)_2 \cdot 4\text{H}_2\text{O}$: -3032.4 ± 1.9 , $\text{Na}_2\text{Mg}(\text{SO}_4)_2 \cdot 4\text{H}_2\text{O}$: -3432.3 ± 1.7 , $\text{Na}_2\text{Co}(\text{SO}_4)_2 \cdot 4\text{H}_2\text{O}$: -3034.4 ± 1.9 , $\text{Na}_2\text{Zn}(\text{SO}_4)_2 \cdot 4\text{H}_2\text{O}$: -3132.6 ± 1.9 , $\text{Na}_2\text{Mn}(\text{SO}_4)_2 \cdot 2\text{H}_2\text{O}$: -2727.3 ± 1.8 . The data allow the stability of these phases to be assessed with respect to Na_2SO_4 , $\text{MSO}_4 \cdot m\text{H}_2\text{O}$ and $\text{H}_2\text{O}(\text{l})$. $\text{Na}_2\text{Ni}(\text{SO}_4)_2 \cdot 4\text{H}_2\text{O}$ is stable with respect to Na_2SO_4 , NiSO_4 and $\text{H}_2\text{O}(\text{l})$ by a significant amount of $\approx 50 \text{ kJ mol}^{-1}$ whereas $\text{Na}_2\text{Mn}(\text{SO}_4)_2 \cdot 2\text{H}_2\text{O}$ is stable with respect to Na_2SO_4 , MnSO_4 and $\text{H}_2\text{O}(\text{l})$ only by $\approx 25 \text{ kJ mol}^{-1}$. The values for the other blödite–kröhnkite phases lie in between. When considering the stability with respect to higher hydrates, the stability margin decreases; for example, $\text{Na}_2\text{Ni}(\text{SO}_4)_2 \cdot 4\text{H}_2\text{O}$ is still stable with respect to Na_2SO_4 , $\text{NiSO}_4 \cdot 4\text{H}_2\text{O}$ and $\text{H}_2\text{O}(\text{l})$, but only by $\approx 20 \text{ kJ mol}^{-1}$. Among the phases studied and chemical reactions considered, the Na–Ni phase is the most stable one, and the Na–Mn, Na–Co, and Na–Cu phases show lower stability.

 Received 8th November 2020
 Accepted 14th December 2020

DOI: 10.1039/d0ra09501j

rsc.li/rsc-advances

1. Introduction

The most common energy storage systems are batteries whose storage capacity surpasses by far mechanical or latent-heat storage systems.¹ Batteries based on lithium were developed and optimized in the last decades² and are used widely in many modern applications. For large-scale grid application, however, their use may be restricted by limited geological reserves of lithium and earth-abundant alternatives are needed. Studies smoothly pass through the development of dual metal ion batteries and hybrid metal ion batteries.³ One of the possible solutions is the development and implementation of batteries based on sodium whose geological reserves are essentially limitless. Such a possibility is being extensively investigated.^{4–7} Some of the phases proposed for use in such batteries are

isostructural with the minerals blödite [nominally $\text{Na}_2\text{Mg}(\text{SO}_4)_2 \cdot 4\text{H}_2\text{O}$] and kröhnkite [nominally $\text{Na}_2\text{Cu}(\text{SO}_4)_2 \cdot 2\text{H}_2\text{O}$].

Thermodynamic stability is one of the criteria for a successful development of commercial batteries. The phases that make up the anodes and cathodes must retain their properties over many redox cycles. Natrochalcite ($\text{Na}[\text{Cu}_2(\text{OH})(\text{H}_2\text{O})(\text{SO}_4)_2]$), as an example, turns amorphous when operating as an anode, but recrystallizes back during the subsequent charge.⁶ H_2O as a component in the batteries may be problematic because sulfates tend to be soluble and reactive towards water.⁸ Hence, anhydrous sulfates may be preferred⁹ but hydrous sulfates are being tested as well.¹⁰ Thermodynamic data suggest which phase assemblage are located energetically downhill and predict if, and with what driving force, the phases of interest for the battery development may tend to convert to other ones.

In this work, we address the question of thermodynamic properties and thermodynamic stability of a series of binary sodium-transition metal sulfates isostructural with blödite or kröhnkite. Some of them were previously tested as precursors for possible use in sodium-based batteries. The thermodynamic data were derived by a combination of acid-solution and relaxation calorimetry. Of particular interest is then the question is the title compounds have a tendency to decompose to simple sulfates.

^aInstitute of Geosciences, Friedrich-Schiller University, Burgweg 11, 07749 Jena, Germany. E-mail: Juraj.Majzlan@uni-jena.de

^bInstitute of General and Inorganic Chemistry, Bulgarian Academy of Sciences, 1113 Sofia, Bulgaria

^cDepartment of Chemistry and Physics of Materials, University of Salzburg, Jakob-Haringer-Strasse 2a, 5020 Salzburg, Austria

† Electronic supplementary information (ESI) available. See DOI: 10.1039/d0ra09501j



2. Crystal structures of blödite and kröhnkite

The crystal structure of blödite [Fig. 1a, nominally $\text{Na}_2\text{-Mg}(\text{SO}_4)_2 \cdot 4\text{H}_2\text{O}$]^{11,12} consists of $[\text{Mg}(\text{SO}_4)_2(\text{H}_2\text{O})_4]^{2-}$ clusters that are interlinked by Na-centered polyhedra and hydrogen bonds. The ionic conductivity of these phases is facilitated by Na ions positioned in channels running along the [100] direction. Apart from Mg^{2+} , the structures of this type could also incorporate divalent Fe, Co, Ni, Zn. The crystal structure of kröhnkite [Fig. 1b, nominally $\text{Na}_2\text{Cu}(\text{SO}_4)_2 \cdot 2\text{H}_2\text{O}$]¹³ is more condensed than that of blödite. It consists of heteropolyhedral chains composed of $\text{CuO}_4(\text{H}_2\text{O})_2$ octahedra and sulfate tetrahedra.^{14,15} In kröhnkite itself, the octahedra are strongly distorted owing to the Jahn–Teller effect but these structures accept other cations that do not have the tendency to distort the octahedra.

3. Experimental section

3.1. Synthesis

Syntheses of the phases investigated in this work were extensively described.^{16–20} The double salts $\text{Na}_2\text{M}^{2+}(\text{SO}_4)_2 \cdot n\text{H}_2\text{O}$ ($\text{M} = \text{Mg, Mn, Co, Ni, Cu, Zn}$ $n = 2$ or 4) were obtained by crystallization from ternary solutions according to the solubility diagrams of the three-component $\text{Na}_2\text{SO}_4\text{-MSO}_4\text{-H}_2\text{O}$ systems at 25 °C. Essentially, saturated high-temperature solutions at about 60–70 °C, were cooled subsequently to 25 °C, thereby forming a solid phase. The suspensions were stirred vigorously for 2 days until complete homogenization and then filtered. The concentration of M^{2+} ions was determined by different titrimetric methods of analysis and by calculations using the method of algebraic indirect identification of solid-phase compositions.

3.2. Characterization

After the syntheses, but also prior to each calorimetric experiment, phase purity of the samples was tested by powder X-ray

Table 1 Lattice parameters of the studied phases

| | <i>a</i> (Å) | <i>b</i> (Å) | <i>c</i> (Å) | β (°) | <i>V</i> (Å ³) |
|---|--------------|--------------|--------------|-------------|----------------------------|
| $\text{Na}_2\text{M}(\text{SO}_4)_2 \cdot 4\text{H}_2\text{O}$, space group $P2_1/a$ | | | | | |
| <i>M</i> = Ni | 11.0373(7) | 8.1870(5) | 5.5302(4) | 100.503(4) | 491.35(6) |
| <i>M</i> = Mg | 11.1295(2) | 8.2459(2) | 5.5412(1) | 100.849(2) | 499.44(2) |
| <i>M</i> = Co | 11.1023(5) | 8.2471(4) | 5.5376(3) | 100.358(3) | 498.77(4) |
| <i>M</i> = Zn | 11.1154(9) | 8.2423(7) | 5.5406(3) | 100.738(5) | 498.72(6) |
| $\text{Na}_2\text{M}(\text{SO}_4)_2 \cdot 2\text{H}_2\text{O}$, space group $P2_1/c$ | | | | | |
| <i>M</i> = Cu^{24} | 5.8054(7) | 12.659(2) | 5.5145(6) | 108.454(6) | 384.42(9) |
| <i>M</i> = Mn | 5.8203(6) | 12.992(2) | 5.4919(6) | 106.076(6) | 399.05(8) |

diffraction (XRD). The data were collected with a Bruker D8 ADVANCE with DAVINCI design, and with Cu $K\alpha$ radiation, Ni filter, and a Lynxeye 1D detector. A step size of 0.02° 2θ and a 0.25 s time per step of were used. Lattice parameters were refined using the JANA2006 program.²¹

3.3. Calorimetric methods

For the solution calorimetric experiments at $T = 25$ °C, we used a commercial IMC-4400 isothermal microcalorimeter (Calorimetry Sciences Corporation) which we modified for the purposes of acid-solution calorimetry.²² The liquid bath of the calorimeter was held at a constant temperature of 298.15 K with fluctuations smaller than 0.0005 K. The calorimetric solvent was 25 g of deionized water or 25 g of 5 N HCl contained in a polyetheretherketone (PEEK) cup with a total volume of 60 mL. The cup was then closed with a PEEK screw lid and inserted into the calorimeter well. The calorimeter stabilized after ≈ 8 hours. During the stabilization and the experiment, the solvent was stirred by a SiO_2 glass stirrer by a motor positioned about 40 cm from the active zone of the instrument. The samples were pressed into a pellet and weighed on a micro-balance with a precision of 0.002 mg (as stated by the manufacturer). The pellets were then dropped through an SiO_2 glass tube into the solvent and the heat produced or consumed during the

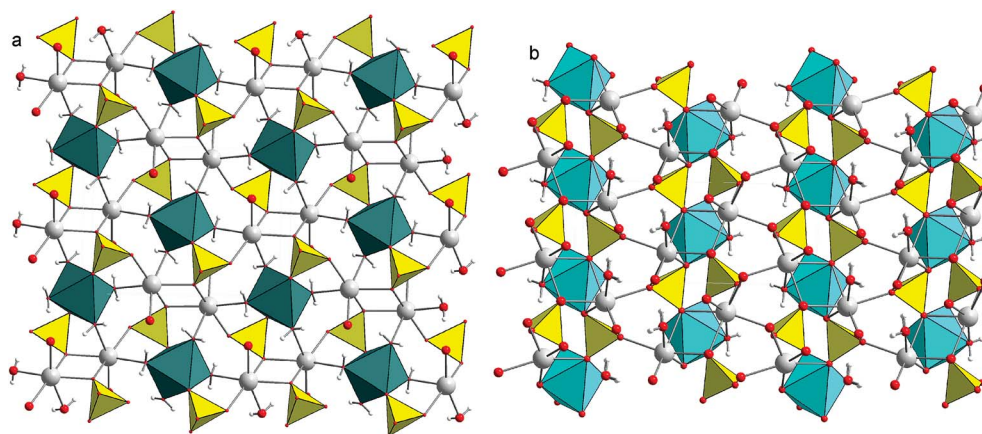


Fig. 1 Crystal structure of (a) blödite (projection onto 001) and (b) kröhnkite (projection onto 100). Cyan octahedra are Cu-centered, deep-green octahedra Mg-centered. Yellow are sulfate tetrahedra, gray balls represent Na, small white balls the H atoms. Red balls represent O atoms, their size reduced when they are a part of a coordination polyhedron. Note the octahedral–tetrahedral chains (parallel to [001]) in the structure of kröhnkite and the cluster of two tetrahedra and an octahedron in the structure of blödite.



dissolution was measured. The heat flow between the reaction cup and the constant temperature reservoir was then integrated to calculate the caloric effect. A typical experiment lasted 50–60 minutes and the end of the experiment was judged from the return of the baseline to the pre-experiment position. The pellet mass of each measured phase was calculated according to the stoichiometry of the thermochemical cycle. Further details on operation, calibration, and accuracy checks can be found in.²²

Heat capacity was measured by relaxation calorimetry using a commercial Physical Properties Measurement System (PPMS, from Quantum Design, San Diego, California) at the University of Salzburg, Austria. With due care, accuracy can be within 1% for 5 K to 300 K, and 5% for 0.7 K to 5 K.²³ Powdered samples were wrapped in a thin Al foil and compressed to produce ≈ 0.5 mm thick pellets, which were then placed onto the sample platform of the calorimeter for measurement.

4. Results

All samples used in this study were crystalline, with sharp peaks in their powder XRD patterns. The refined lattice parameters are summarized in Table 1. The structures corresponded to the structures previously determined for the minerals blödite¹² and

kröhnkite.²⁵ The starting models for the full-profile fits were taken from these publications.

Enthalpies of dissolution in 5 N HCl, measured by acid-solution calorimetry, were converted to enthalpies of formation *via* the appropriate thermochemical cycles (Table 2). A suite of simple metal sulfates, metal oxides, and Na₂SO₄ were used as reference phases in this process.²² The dissolution of all samples was rapid and no problems were encountered during the calorimetric experiments.

Low-temperature heat capacities (C_p) were measured from 2 up to 310 K and the raw data is presented in Tables S1–Sx.† The data were fit with a set of polynomials. At low temperatures ($T < 18$ K), the extended Debye polynomial $C_p = A_3T^3 + A_5T^5$ was used for Na₂M(SO₄)₂· n H₂O with M = Co, Mg, Zn. For M = Mn and Ni, the C_p data showed low-temperature anomalies centered at 2.5 and 2.6 K, respectively (Fig. 2). These anomalies are related most likely to the magnetic properties of Mn²⁺ and Ni²⁺. Because of the low temperatures at which they are located, a full shape of the C_p anomalies was not determined. In this region for M = Mn and Ni, we used polynomials $C_p = \sum A_p T^p$ (with $p = 1$ –6) for the fits. There is an additional, very small C_p anomaly at $T = 15.2$ in the data for M = Mn whose nature is not clear. At higher temperatures, several orthogonal polynomials $C_p =$

Table 2 Thermochemical cycles for the studied phases with the enthalpy values measured or used in these cycles. All values in kJ mol⁻¹

| | |
|---|------|
| $\text{Na}_2\text{M}(\text{SO}_4)_2 \cdot n\text{H}_2\text{O} = 2\text{Na}^+ + \text{M}^{2+} + 2\text{SO}_4^{2-} + n\text{H}_2\text{O}$ | (1) |
| $\text{Na}_2\text{SO}_4 = 2\text{Na}^+ + \text{SO}_4^{2-}$ | (2) |
| $\text{MSO}_4 \cdot m\text{H}_2\text{O} = \text{M}^{2+} + \text{SO}_4^{2-} + m\text{H}_2\text{O}$ | (3) |
| $\text{MO} + 2\text{H}^+ = \text{M}^{2+} + \text{H}_2\text{O}$ | (4) |
| $\text{H}_2\text{O}(\text{l}) = \text{H}_2\text{O}(\text{aq.})$ | (5) |
| $2\text{Na} + \text{S} + 2\text{O}_2 = \text{Na}_2\text{SO}_4$ | (6) |
| $\text{M} + \text{S} + (2 + m/2)\text{O}_2 + m\text{H}_2 = \text{MSO}_4 \cdot m\text{H}_2\text{O}$ | (7) |
| $\text{M} + (1/2)\text{O}_2 = \text{MO}$ | (8) |
| $\text{H}_2 + (1/2)\text{O}_2 = \text{H}_2\text{O}$ | (9) |
| $2\text{Na} + \text{M} + 2\text{S} + (4 + n/2)\text{O}_2 + n\text{H}_2 = \text{Na}_2\text{M}(\text{SO}_4)_2 \cdot n\text{H}_2\text{O}$ | (10) |

For a thermodynamic cycle closed with the simple metal sulfate (MSO₄· m H₂O, M = Mg, Ni, Co, Cu): $\Delta H_{10} = \Delta_f H^\circ = -\Delta H_1 + \Delta H_2 + \Delta H_3 + (n-m)\Delta H_5 + \Delta H_6 + \Delta H_7 + (n-m)\Delta H_9$

For a thermochemical cycle closed with the metal oxide (MO, M = Mn, Zn), MgSO₄, and MgO: $\Delta H_{10} = \Delta_f H^\circ = -\Delta H_1 + \Delta H_2 + \Delta H_{3,\text{MgSO}_4} + \Delta H_{4,\text{MO}} + n\Delta H_5 - \Delta H_{4,\text{MgO}} + \Delta H_6 + \Delta H_{7,\text{MgSO}_4} + \Delta H_{8,\text{MO}} + n\Delta H_9 - \Delta H_{8,\text{MgO}}$

Dissolution/dilution enthalpies

$$\begin{aligned} \Delta H_{1,\text{Co}} &= \Delta_{\text{sol}}H[\text{Na}_2\text{Co}(\text{SO}_4)_2 \cdot 4\text{H}_2\text{O}] = 51.62 \pm 0.31(6) \\ \Delta H_{1,\text{Cu}} &= \Delta_{\text{sol}}H[\text{Na}_2\text{Cu}(\text{SO}_4)_2 \cdot 2\text{H}_2\text{O}] = 54.18 \pm 0.38(4) \\ \Delta H_{1,\text{Mg}} &= \Delta_{\text{sol}}H[\text{Na}_2\text{Mg}(\text{SO}_4)_2 \cdot 4\text{H}_2\text{O}] = 42.21 \pm 0.21(5) \\ \Delta H_{1,\text{Mn}} &= \Delta_{\text{sol}}H[\text{Na}_2\text{Mn}(\text{SO}_4)_2 \cdot 2\text{H}_2\text{O}] = 37.97 \pm 0.17(5) \\ \Delta H_{1,\text{Ni}} &= \Delta_{\text{sol}}H[\text{Na}_2\text{Ni}(\text{SO}_4)_2 \cdot 4\text{H}_2\text{O}] = 49.27 \pm 0.15(6) \\ \Delta H_{1,\text{Zn}} &= \Delta_{\text{sol}}H[\text{Na}_2\text{Zn}(\text{SO}_4)_2 \cdot 4\text{H}_2\text{O}] = 65.22 \pm 0.17(5) \\ \Delta H_2 &= \Delta_{\text{sol}}H(\text{Na}_2\text{SO}_4) = 21.08 \pm 0.14(6) \\ \Delta H_{3,\text{Co}} &= \Delta_{\text{sol}}H(\text{CoSO}_4 \cdot 7\text{H}_2\text{O}) = 44.66 \pm 0.31(6) \\ \Delta H_{3,\text{Cu}} &= \Delta_{\text{sol}}H(\text{CuSO}_4 \cdot 5\text{H}_2\text{O}) = 49.71 \pm 0.19(17) \\ \Delta H_{3,\text{Mg}} &= \Delta_{\text{sol}}H(\text{MgSO}_4) = -53.50 \pm 0.48(7) \\ \Delta H_{3,\text{Ni}} &= \Delta_{\text{sol}}H(\text{NiSO}_4 \cdot 7\text{H}_2\text{O}) = 41.26 \pm 0.58(9) \\ \Delta H_{4,\text{Mg}} &= \Delta_{\text{sol}}H(\text{MgO}) = -149.68 \pm 0.60(9) \\ \Delta H_{4,\text{Mn}} &= \Delta_{\text{sol}}H(\text{MnO}) = -113.35 \pm 0.05(3) \\ \Delta H_{4,\text{Zn}} &= \Delta_{\text{sol}}H(\text{ZnO}) = -70.24 \pm 0.11(4) \\ \Delta H_5 &= \Delta_{\text{dilution}}H = -0.54 \end{aligned}$$

Formation enthalpies

$$\begin{aligned} \Delta H_6 &= \Delta_f H^\circ(\text{Na}_2\text{SO}_4) = -1387.8 \pm 0.4 \text{ (ref. 26)} \\ \Delta H_{7,\text{Co}} &= \Delta_f H^\circ(\text{CoSO}_4 \cdot 7\text{H}_2\text{O}) = -2979.3 \pm 1.5 \text{ (ref. 27)} \\ \Delta H_{7,\text{Cu}} &= \Delta_f H^\circ(\text{CuSO}_4 \cdot 5\text{H}_2\text{O}) = -2279.5 \pm 3.4 \text{ (ref. 27)} \\ \Delta H_{7,\text{Mg}} &= \Delta_f H^\circ(\text{MgSO}_4) = -1288.64 \pm 1.28 \text{ (ref. 28)} \\ \Delta H_{7,\text{Ni}} &= \Delta_f H^\circ(\text{NiSO}_4 \cdot 7\text{H}_2\text{O}) = -2976.8 \pm 1.5 \text{ (ref. 27)} \\ \Delta H_{8,\text{Mg}} &= \Delta_f H^\circ(\text{MgO}) = -601.6 \pm 0.3 \text{ (ref. 26)} \\ \Delta H_{8,\text{Mn}} &= \Delta_f H^\circ(\text{MnO}) = -385.2 \pm 0.5 \text{ (ref. 26)} \\ \Delta H_{8,\text{Zn}} &= \Delta_f H^\circ(\text{ZnO}) = -350.5 \pm 0.3 \text{ (ref. 26)} \\ \Delta H_9 &= \Delta_f H^\circ(\text{H}_2\text{O}, \text{l}) = -285.8 \pm 0.1 \text{ (ref. 26)} \end{aligned}$$



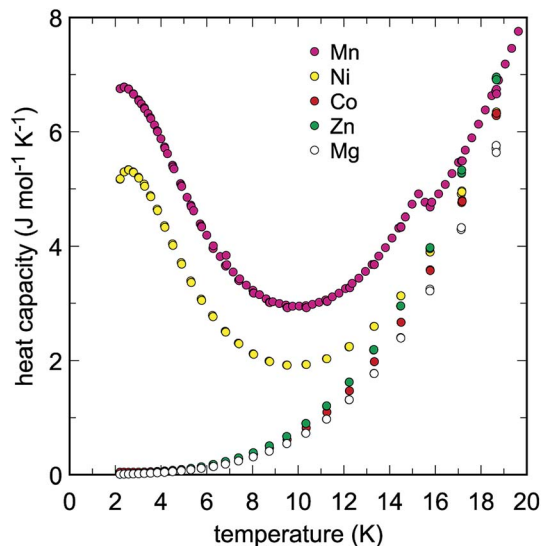


Fig. 2 Low-temperature heat capacity of the studied $\text{Na}_2\text{M}(\text{SO}_4)_2 \cdot n\text{H}_2\text{O}$ phases. Note the C_p anomalies in the data for $M = \text{Ni}$ and Mn .

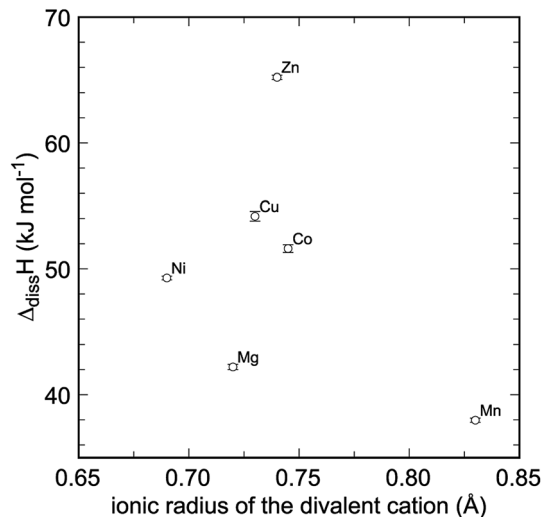


Fig. 3 Enthalpies of dissolution ($\Delta_{\text{diss}}H$) for the studied $\text{Na}_2\text{M}(\text{SO}_4)_2 \cdot n\text{H}_2\text{O}$ phases in 5 N HCl.

$\Sigma A_p T^p$ (with $p = 0-8$ or $0-9$) were used. The polynomials were joined and used for the determination of thermodynamic functions between 0–300 K. The results, including values of smoothed C_p and entropy at evenly spaced temperature intervals, are listed in Tables S1–S10.†

The enthalpies of formation and entropies of formation (Table 3) were used to calculate Gibbs free energies of formation. Auxiliary data needed for these calculations (entropies of elements in their standard state) were taken from ref. 26.

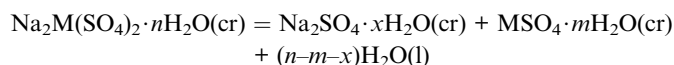
5. Discussion

The enthalpies of dissolution of the title compounds in 5 N HCl are endothermic, with small magnitude (Table 2), as expected for hydrated sulfates. They show no linear correlation between the ionic radii (IR) of the divalent metals (Fig. 3), as reported for similar Li phases.²⁹ With the exception of Mn^{2+} (IR = 0.83 Å), the ionic radii of the divalent metals considered here are fairly similar to each other. We assume that a simple relationship²⁹ is obscured by the structural variations between the blödite- and kröhnkite-like sulfates. In addition, the introduction of H_2O molecules in these structures induces structural depolymerization, as opposed to the anhydrous phases. Such depolymerization can allow relaxation of the structures and flexibility in

the uptake of various divalent cations to a certain extent. Detailed studies^{16–20} showed that mixing is severely limited in many solid solutions of these phases and, therefore, the flexibility is also limited.

There is no simple (*i.e.*, linear) relationship between the chemical composition and formation enthalpies or Gibbs free energies. To decipher such relationship, detailed studies of the electronic structure of the title compounds, using *ab initio* calculations, may be needed. Such calculations are, however, beyond the scope of this contribution. Even though the question of interplay of crystal structures and thermodynamic properties is intriguing and recurring, this study cannot provide satisfactory answers to it.

Gibbs free energies of formation (Table 3) allow to evaluate the stability of the title phases quantitatively with respect to the simple sulfates. Considering the reaction



A set of equilibria can be evaluated. If the batteries should be operated with such phases, the presence of additional free water (aqueous solution) is unlikely. The implication for this reaction is that $m < n$, and hence higher hydrates are not considered in

Table 3 Summary of thermodynamic data for the $\text{Na}_2\text{M}(\text{SO}_4)_2 \cdot n\text{H}_2\text{O}$ phases from this study

| | $\Delta_f H^\circ$ kJ mol ⁻¹ | S° J mol ⁻¹ K ⁻¹ | $\Delta_f S^\circ$ J mol ⁻¹ K ⁻¹ | $\Delta_f G^\circ$ kJ mol ⁻¹ |
|--|---|---|--|---|
| $\text{Na}_2\text{Ni}(\text{SO}_4)_2 \cdot 4\text{H}_2\text{O}$ | -3492.5 ± 1.7 | 407.3 ± 2.9 | -1543.2 ± 2.9 | -3032.4 ± 1.9 |
| $\text{Na}_2\text{Mg}(\text{SO}_4)_2 \cdot 4\text{H}_2\text{O}$ | -3896.4 ± 1.5 | 396.7 ± 2.8 | -1556.6 ± 2.8 | -3432.3 ± 1.7 |
| $\text{Na}_2\text{Co}(\text{SO}_4)_2 \cdot 4\text{H}_2\text{O}$ | -3494.0 ± 1.6 | 409.3 ± 2.9 | -1541.4 ± 2.9 | -3034.4 ± 1.9 |
| $\text{Na}_2\text{Zn}(\text{SO}_4)_2 \cdot 4\text{H}_2\text{O}$ | -3588.9 ± 1.7 | 431.8 ± 3.0 | -1530.5 ± 3.1 | -3132.6 ± 1.9 |
| $\text{Na}_2\text{Cu}(\text{SO}_4)_2 \cdot 2\text{H}_2\text{O}^{24}$ | -2791.7 ± 3.5 | 315.5 ± 3.8 | -1171.8 ± 3.8 | -2442.3 ± 3.6 |
| $\text{Na}_2\text{Mn}(\text{SO}_4)_2 \cdot 2\text{H}_2\text{O}$ | -3066.8 ± 1.7 | 347.4 ± 2.4 | -1138.7 ± 2.5 | -2727.3 ± 1.8 |



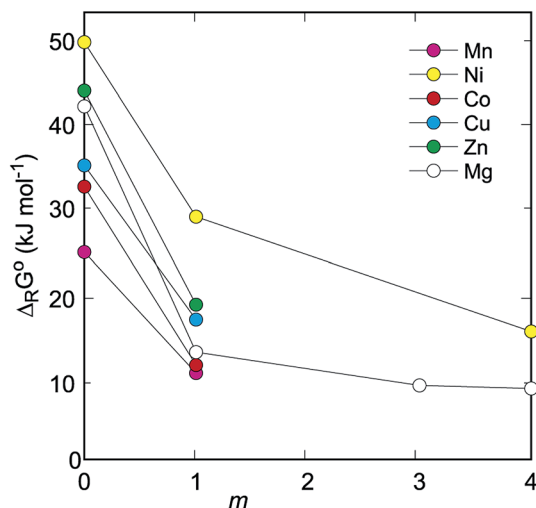


Fig. 4 Gibbs free energies of decomposition ($\Delta_{\text{R}}G^{\circ}$) of $\text{Na}_2\text{M}(\text{SO}_4)_2 \cdot n\text{H}_2\text{O}$ to simple sulfates. The reaction considered is $\text{Na}_2\text{M}(\text{SO}_4)_2 \cdot n\text{H}_2\text{O}(\text{cr}) \rightarrow \text{Na}_2\text{SO}_4 \cdot x\text{H}_2\text{O}(\text{cr}) + \text{MSO}_4 \cdot m\text{H}_2\text{O}(\text{cr}) + (n-m-x)\text{H}_2\text{O}(\text{l})$. For all reactions considered, $x = 0$ and $n = 2$ or 4 , as specified in Tables 1 and 3. The uncertainties are smaller than the symbols. The lines that connect the individual points are only guides to the eye.

these calculations. For consistency, all Gibbs free energies of formation ($\Delta_{\text{f}}G^{\circ}$) for the transition-metal sulfates were taken from ref. 30, even though the thermodynamic data for some systems have been updated since then, e.g.,²⁷ The $\Delta_{\text{f}}G^{\circ}$ value for $\text{CoSO}_4 \cdot \text{H}_2\text{O}$ was corrected because the values of formation enthalpy and entropy, listed by,³⁰ do not add up to her $\Delta_{\text{f}}G^{\circ}$ for this phase. The $\Delta_{\text{f}}G^{\circ}$ values for magnesium sulfates were adopted from ref. 31 that for Na_2SO_4 from ref. 26.

The $\Delta_{\text{R}}G^{\circ}$ values for this reaction are graphically shown for all $\text{Na}_2\text{M}(\text{SO}_4)_2 \cdot n\text{H}_2\text{O}(\text{cr})$ phases in Fig. 4. We note that these values are approximate as only pure $\text{H}_2\text{O}(\text{l})$ is considered. As mentioned above, the Na–M sulfates are highly soluble and aqueous solutions, if present, would likely have high ionic strength and affect the equilibria. Because of the uncertainties regarding the composition of such solutions and the appropriate activity-molality models, calculations involving aqueous solutions with Na, M, and sulfate as solutes were not performed here.

6. Conclusions

All $\text{Na}_2\text{M}(\text{SO}_4)_2 \cdot n\text{H}_2\text{O}$ phases are stable with respect to the assemblages of Na_2SO_4 , $\text{MSO}_4 \cdot m\text{H}_2\text{O}$, and $\text{H}_2\text{O}(\text{l})$. However, the differences among the $\text{Na}_2\text{M}(\text{SO}_4)_2 \cdot n\text{H}_2\text{O}$ phases with different M^{2+} cations are significant. When considering their stability with respect to Na_2SO_4 , MSO_4 , and $\text{H}_2\text{O}(\text{l})$, the Gibbs free energies vary from $\approx 25 \text{ kJ mol}^{-1}$ for $\text{M} = \text{Mn}$ up to $\approx 50 \text{ kJ mol}^{-1}$ for $\text{M} = \text{Ni}$. The differences, although smaller in magnitude, remain also for higher sulfates ($\text{MSO}_4 \cdot m\text{H}_2\text{O}$). For the tetrahydrates ($\text{MSO}_4 \cdot 4\text{H}_2\text{O}$), the difference between $\text{M} = \text{Ni}$ and $\text{M} = \text{Mg}$ is only $\approx 7 \text{ kJ mol}^{-1}$ (Fig. 4). Hence, the thermodynamic calculations document the stability of the $\text{Na}_2\text{-M}(\text{SO}_4)_2 \cdot n\text{H}_2\text{O}$ phases. They also show that the stability margin

is relatively small. Should the $\text{Na}_2\text{M}(\text{SO}_4)_2 \cdot n\text{H}_2\text{O}$ phases be decomposed during desodiation cycles, the driving force for the re-assembling of their structures is small and their recrystallization, similar to that observed for natrochalcite,⁶ could be problematic. From the set investigated here, the $\text{Na}_2\text{Ni}(\text{SO}_4)_2 \cdot 4\text{H}_2\text{O}$ phase is the most stable one with respect to the simple sulfates. If $\text{Na}_2\text{Fe}(\text{SO}_4)_2 \cdot 2\text{H}_2\text{O}$ should turn out as a promising candidate for the sodium batteries,^{7,10} the stability of the dihydrate with $\text{M} = \text{Ni}$ should be also explored with respect to the stabilization of the materials in the batteries.

Conflicts of interest

The authors declare no conflict of interest.

References

- 1 M. A. Hannan, M. M. Hoque, A. Mohamed and A. Ayob, *Renewable Sustainable Energy Rev.*, 2017, **69**, 771.
- 2 M. Li, J. Lu, Z. Chen and K. Amine, *Adv. Mater.*, 2018, **30**, 1800561.
- 3 R. Stoyanova, V. Koleva and A. Stoyanova, *Chem. Rec.*, 2019, **19**, 474.
- 4 M. Reynaud, M. Ati, S. Boulineau, M. T. Sougrati, B. C. Melot, G. Rousse, J. N. Chotard and J. M. Tarascon, *ECS Trans.*, 2013, **50**, 11.
- 5 C. Masquelier and L. Croguennec, *Chem. Rev.*, 2013, **113**, 6552.
- 6 Z. Liu, H. J. Zhou, S. S. Ang and J. J. Zhang, *Electrochim. Acta*, 2016, **211**, 619.
- 7 T. Watcharatharapong, J. T. Thienprasert, S. Chakraborty and R. Ahuja, *Nano Energy*, 2019, **55**, 123.
- 8 T. Jin, H. Li, K. Zhu, P.-F. Wang, P. Liu and L. Jiao, *Chem. Soc. Rev.*, 2020, **49**, 2342.
- 9 P. Barpanda, G. Oyama, S. Nishimura, S.-C. Chung and A. Yamada, *Nat. Commun.*, 2014, **5**, 4358.
- 10 P. Barpanda, G. Oyama, C. D. Ling and A. Yamada, *Chem. Mater.*, 2014, **26**, 1297.
- 11 M. Giglio, *Acta Crystallogr.*, 1958, **11**, 789.
- 12 F. C. Hawthorne, *Can. Mineral.*, 1985, **23**, 669.
- 13 B. Dahlman, *Ark. Mineral. Geol.*, 1952, **1**, 339–366.
- 14 M. Fleck, U. Kolitsch and B. Hertweck, *Z. Kristallogr.*, 2002, **217**, 435.
- 15 U. Kolitsch and M. Fleck, *Eur. J. Mineral.*, 2006, **18**, 471.
- 16 M. Georgiev, T. Bancheva, D. Marinova, R. Stoyanova and D. Stoilova, *International Journal of Scientific Research in Science and Technology*, 2016, **2**, 279.
- 17 M. Georgiev, D. Marinova, T. Bancheva and D. Stoilova, *J. Chem. Technol. Metall.*, 2017, **52**, 902.
- 18 D. Marinova, M. Georgiev, T. Bancheva and D. Stoilova, *International Journal of Scientific Research in Science and Technology*, 2016, **2**, 283.
- 19 D. Marinova, M. Georgiev, T. Bancheva, R. Stoyanova and D. Stoilova, *J. Therm. Anal. Calorim.*, 2017, **130**, 1925.
- 20 D. Marinova, M. Wildner, T. Bancheva, R. Stoyanova, M. Georgiev and D. G. Stoilova, *Phys. Chem. Miner.*, 2018, **45**, 801.



- 21 V. Petříček, M. Dušek and L. Palatinus, *Z. Kristallogr.*, 2014, **229**, 345.
- 22 J. Majzlan, *Acta geol. Slovaca*, 2017, **9**, 171.
- 23 C. A. Kennedy, M. Stancescu, R. A. Marriott and M. A. White, *Cryogenics*, 2007, **47**, 107.
- 24 J. Majzlan, A. Zittlau, K. D. Grevel, J. Schliesser, B. F. Woodfield, E. Dachs, M. Števkó, J. Plášil and S. Milovská, *Can. Mineral.*, 2015, **53**, 937.
- 25 F. C. Hawthorne and R. B. Ferguson, *Acta Crystallogr., Sect. B: Struct. Crystallogr. Cryst. Chem.*, 1975, **31**, 1753.
- 26 R. A. Robie and B. S. Hemingway, *United States Geol. Surv. Bull.*, 1995, **2131**, 461.
- 27 K. D. Grevel and J. Majzlan, *Chem. Geol.*, 2011, **286**, 301.
- 28 R. J. Lemire, D. A. Palmer, P. Taylor and H. Schlenz, *Chemical Thermodynamics of Iron, Part 2*. OECD Nuclear Energy Agency, 2020, p. 921.
- 29 A. V. Radha, L. Lander, G. Rousse, J. M. Tarascon and A. Navrotsky, *J. Mater. Chem. A*, 2015, **3**, 2601.
- 30 C. W. DeKock, *Information Circular*, Bureau of Mines, 1982, 8910, p. 45.
- 31 K. D. Grevel and J. Majzlan, *Geochim. Cosmochim. Acta*, 2009, **73**, 6805.

